Serendipitous Internal Wave Signals in Deep Argo Data

Gregory C. Johnson[1], Caitlin B. Whalen[2], Sarah G. Purkey[3], and Nathalie Zilberman[3]

[1]*NOAA/Pacific Marine Environmental Laboratory, Seattle, Washington 98115, USA*

[2]*Applied Physics Laboratory, University of Washington, Seattle, Washington, 98105, USA*

[3]*Scripps Institution of Oceanography, UC San Diego, La Jolla, California, 92093, USA*

Key points:

- Engineering data of Deep SOLO float descent rates serendipitously reveal vertical velocity signatures of internal waves

- Deep internal wave vertical velocities have typical sinusoidal amplitudes of 0.007 dbar s^{-1} and vertical wavelengths of ~400–1600 dbar

- Vertical velocity variances and dominant vertical wavelengths exhibit geographical patterns, varying among and within deep ocean basins

Abstract Serendipitous measurements of deep internal wave signatures are evident in variations in the descent rates of certain Deep Argo floats (Deep SOLO models), which oscillate around a slow decrease with increasing pressure (and density). Averaged from 1000 dbar to the seafloor (using 10070 profiles that extend to at least 3000 dbar, and sometimes as deep as 6000 dbar) the mean of vertical velocity variances corresponds to a sinusoidal wave amplitude of about 0.007 dbar s^{-1}. The distribution of variances is skewed towards larger values. They also exhibit notable regional variations among and within some deep ocean basins, with generally larger variances in regions of rougher topography or stronger deep currents. Dominant vertical wavelengths estimated from Morlet wavelet transform power spectra range from 393 to 1572 dbar, most frequently 786 and 935 dbar. Vertical wavelengths are weakly anticorrelated with bathymetric roughness, expectedly since shorter wavelengths should be found near generation regions.

Plain Language Summary Ocean density increases with increasing depth, supporting internal waves below the ocean surface. These internal waves are generated near the surface by unsteady wind forcing such as passing storms and

near the bottom by interactions of currents (including tidal) with rough topography. They can carry energy for long distances in both the vertical and the horizontal. When they break, they play important roles in mixing temperature, salinity, and other water properties. Deep Argo is an observing system designed to measure temperature and salinity profiles from the surface to the bottom of the ocean. One model of deep Argo float serendipitously observes internal wave signals as perturbations in its descent rate, which it records primarily for navigation purposes, from the surface to the ocean floor. These observations reveal patterns in the magnitudes of these internal wave signals, with stronger internal wave activity near rough topography such as continental rises and mid-ocean ridges and lower levels over smoother abyssal plains. Also, regions with strong deep flows, such as the Samoan Passage through which bottom water is funneled into the North Pacific, or the region south of the Campbell Plateau through which the Antarctic Circumpolar Current flows, exhibit stronger deep internal wave signatures.

. Introduction

Internal waves are nearly ubiquitous in the oceans (Garrett & Munk, 1979), carrying energy vertically from the surface downward and from the sea-floor upward, as well as horizontally, in some instances over ocean basin-scale distances. Internal wave breaking ultimately dissipates much of the wind and tidal energy in the oceans (Waterhouse et al., 2014; Kunze, 2017), and deep internal wave mixing drives water-mass transformations important to the global deep ocean circulation, sometimes called the meridional overturning circulation (Munk & Wunsch, 1998; de Lavergne et al., 2016; Kunze, 2017; Nikurashin & Ferrari, 2013). Internal waves are often measured either from time series of isotherms (analyzing their vertical displacements or vertical strain) and horizontal velocity (analyzing the velocities or vertical shear of those velocities) (e.g., Alford et al., 2016). Here we use engineering data from the descent portion of Deep Argo float cycles to assess the amplitude of vertical velocities and vertical wavelengths of internal waves in the water column below the thermocline.

Deep Argo is a relatively new mission for the Argo program, designed to regularly sample the global ocean below the 2000-dbar pressure limit of core Argo floats, and hence improve monitoring of variations in ocean temperature, salinity, and currents (Johnson et al., 2015). Floats capable of profiling to 4000 dbar and 6000 dbar have been designed and successfully deployed in regional pilot arrays (Roemmich et al., 2019), quantifying recent warming of bottom waters of Antarctic origin in the Southwest Pacific (Johnson et al., 2019) and Brazil Basins (Johnson et al., 2020), detecting temperature-salinity variability near Antarctic Bottom Water formation regions (Thomas et al., 2020; Foppert et al., 2021), and allowing detailed analyses of deep ocean circulation (Zilberman et al., 2020). A 6000-dbar profiling capability allows sampling from the ocean surface to the sea floor over 98% of the ocean area and 97% of the ocean volume, with the exceptions being a few very deep ocean trenches, and small portions of the ocean immediately above the deepest abyssal plains.

At the start of its descent phase, the Deep SOLO float model (Roemmich et al., 2019) pumps all of the oil that is required to target a 0.05 m s^{-1} descent rate when it reaches the bottom from its external bladder to its internal reservoir. Hence, it sinks most rapidly (order 0.25 m s^{-1}) in the lightest waters near the surface, and steadily slows as it descends into denser waters. Since it does not make buoyancy adjustments during descent, unlike some other profiling floats, a flight model (e.g„ Cusack et al., 2017) is not needed to interpret variations around the background profiling rate as oceanic vertical velocities. The float controller, batteries, and buoyancy engine are inside mated 13" diameter glass hemispheres protected by plastic hard-hat housings, with the CTD (conductivity-temperature-depth) instrument in a smaller externally mounted titanium cylinder. Pressure samples are taken typically at between 5 and 50-dbar pressure intervals, depending on software settings, to monitor the descent rate. A 3-meter wire rope dangling from the float brakes its descent as the rope lays down on the bottom, preventing the instruments on the float from contacting the sea floor.

Initial examinations of vertical descent velocities from Deep SOLO float profiles readily revealed signatures of internal waves as oscillations around what would have otherwise been a steady deceleration with increasing pressure. The float-measured oscillations have average amplitudes of order 0.007 dbar s^{-1} and vertical wavelengths from ~400–1600 dbar in the water column below 1000 dbar. Here we explore regional variations in the amplitudes and wavelengths of these serendipitous observations of internal wave signals among and within the basins sampled by Deep Argo regional pilot arrays using Deep SOLO floats.

2. Data and Methods

Deep SOLO floats measure pressure and time during descent nominally at 5 to 50 dbar intervals, depending on how engineering parameters are set for an individual float. These measurements are telemetered to shore as part of the engineering data when the float surfaces during each nominally 10-day cycle, and reported in Argo trajectory (.traj) files. We only use these data from profiles that sample to at least 2995 dbar, and limit our analysis of the data to pressures greater than 800 dbar, below the main pycnocline in the regions analyzed. We also remove three profiles with vertical gaps in these engineering data that are too long to smooth over. The screening results in 10070 profiles in total, mostly in the Brazil Basin of the western South Atlantic and the Southwest Pacific Basin, but also in the South Australian Basin, the Australian-Antarctic Basin, the North American Basin (western north Atlantic), and a few in the Central and Northeast Pacific basins (Figure 1).

For each profile extending to at least 2995 dbar we estimate vertical velocities from first differences of pressures divided by those of times. We discard the three deepest estimates to avoid bottom interactions, then apply a loess smoother (Cleveland & Devlin, 1988) with a half-power point of ~150 dbar to estimate vertical velocities on a regular grid at 10-dbar intervals from 1000 dbar to the deepest pressure (rounded down to the closest 10 dbar value shallower than

that pressure). We then fit a second-order polynomial to these gridded vertical velocities as an estimate of the background fall rate that steadily decreases with increasing pressure, and subtract those background fall rates from each profile to yield the residual vertical velocities (hereafter w') relative to the background fall rates. Typical background fall rates are about 0.17 ($\pm$0.01) dbar s^{-1} at 1000 dbar, and decrease nearly linearly to about 0.07 ($\pm$0.01) dbar s^{-1} at profile maximum pressures, where the uncertainties (here and throughout the manuscript) are one standard deviation.

We calculate the mean deep w' variances averaged from 1000 dbar to the maximum pressure analyzed for each profile (Figure 2a). We also apply a Morlet wavelet transform (Torrence & Compo, 1998) to each profile to estimate the dominant vertical wavelength of w' (Figure 2b). We define this dominant vertical wavelength as the location of the maximum value of the wavelet power spectrum of w' for all vertical wavelengths and pressures not influenced by zero-padding edge effects (i.e., heeding the "cone of influence").

We look at the correlation of the mean deep w' variances and dominant vertical wavelengths with local bottom topographic roughness. To do that we compute the variance of ocean bathymetry (GEBCO Compilation Group, 2021) at 1' resolution within 40-km square bins on a 0.25° x 0.25° grid and use the resulting map to interpolate roughness to float locations.

3. Results

Mean deep w' variances for all 10070 profiles (computed from 1000 dbar to their deepest gridded pressure, at least 2995 dbar, typically within ~45 dbar of the seafloor) have an average value of 0.23 ($\pm$0.16) $\times$ 10^{-4} dbar^{-2} s^{-2}. However, the mean deep w' variances are not normally distributed (Figure 3a), with 3% of the values falling below the mean minus one standard deviation and 10% of the values falling above the mean plus one standard deviation. The median value of 0.20 $\times$ 10^{-4} dbar^{-2} s^{-2} is somewhat less than the mean value. The mean value corresponds to an idealized sinusoidal disturbance for w' over the entire pressure range with an amplitude of 0.007 dbar s^{-1}. The largest local amplitudes of w' generally do not exceed 0.02 dbar s^{-1}. Hence, the example shown (Figure 2) exhibits a signal with an amplitude towards the high end of the distribution.

The vertical wavelengths of w' at the maximum power of the w' Morlet wavelet spectrum, hereafter referred to as the dominant vertical wavelengths, (e.g., Figure 3b) have an average value of 890 ($\pm$290) dbar. Half of these values are 786 dbar or less, with less than 1% falling below 393 dbar, and half are 935 dbar or greater, with 6% at the maximum possible value of 1572 dbar. This distribution should be regarded with some caution, both because of potential biases resulting from slow profiling through propagating waves noted in the discussion section and because a segment 2.7 times the vertical wavelength is required for that wavelength to be free of the cone of influence (where zero-padding effects bias the power spectrum) even at the mid-point of the portion of the profile analyzed. Using the 46% of the profiles that extend to at least 5250 dbar, and hence can

4

resolve a maximum vertical wavelength of 1572 dbar at their mid-point, results in an average value of 970 ($\pm$300) dbar for the dominant vertical wavelengths. This increase in wavelength is only 9% over the average value using the entire data set.

The geographic distributions of mean deep w' variances (Figure 4) and dominant vertical wavelengths (Figure 5) both exhibit physically sensible patterns among basins and within some individual basins.

The mean deep w' variances (Figure 4) are generally lower than average for the profiles in the North American Basin of the western North Atlantic Ocean, with a few higher values adjacent to the Caribbean Islands. Offshore, the abyssal plain there is very smooth and so these low variances might be anticipated. The dominant vertical wavelengths there are noticeably longer than average (Figure 5). These two features are consistent with little local generation or scattering of internal waves at rough topographic features and propagation of internal waves generated elsewhere from a long distance. The internal wave energy level in regions with little local generation would be expected to be lower, even for the longer vertical wavelength packets that survive traveling from remote generation regions. The few bins with higher variances and smaller wavelengths near the continental slope may result from local interactions between currents and the bathymetry there.

In the Brazil Basin of the western South Atlantic deep w' variance values are largest and vertical wavelengths the smallest near the internal wave generation sites along the rough topography of the Mid-Atlantic Ridge. In contrast, over the smoother abyssal plain in the west far from internal wave generation regions the mean w' variance values are lower and the vertical wavelengths are longer, suggesting that there are very few locally generated internal waves, leaving only low-mode internal waves that may have been generated elsewhere. This pattern is consistent with previous observations of a ridge-to-basin gradient in mixing in the Brazil Basin (Polzin et al., 1997) and with strain and shear variances from WOCE section data in many basins (Kunze et al., 2006). Further west, approaching the continental slope, wavelengths become shorter while the variance remains small, suggesting that while there is little local generation, the continental slope may be reflecting or scattering internal waves, a pattern consistent with modeling studies of the internal wave lifecycle (e.g., de Lavergne et al., 2019). The shorter wavelengths near the slope could also arise at least partly owing to the shorter profiles taken there not resolving the energy at longer wavelengths. In the Argentine Basin vertical wavelengths are small and the deep w' variance is moderate to strong, consistent with the deep-reaching eddies and currents in the region (e.g., Fu, 2007) interacting with the internal wave field in a variety of ways including acting as a conduit for surface-generated internal waves (Danioux et al., 2008; Kunze, 1985; Young & BenJelloul, 1997), or causing a substantial reduction in the internal wave length scales via interactions with the currents vorticity or horizontal strain (Fer et al., 2018; Kunze, 1995).

The mean deep w' variances (Figure 4) in the South Australian and Australian-

Antarctic basins of the far eastern Indian Ocean are generally lower than average, especially in smooth regions of the basins, with some high values and shorter dominant vertical wavelengths (Figure 5) closer to topographic features. Just to the east, profiles south of the Campbell Plateau in the South Pacific have relatively high mean deep w' variances and a variety of dominant vertical wavelengths. The deep-reaching Antarctic Circumpolar Current flows eastward through this region after transiting some very rough bathymetry to the west. Deep-reaching meanders and eddies of that current generating lee waves when flowing over that topography (Cusack et al., 2017; Waterman et al., 2013) may be responsible for some of those high variances.

In the Southwest Pacific Basin, mean deep w' variances (Figure 4) are close to average in many locations, with higher values adjacent to the steep bathymetry of the Tonga-Kermadec Ridge and Trench system and around regions with rough bathymetry including the chain of seamounts comprising the Louisville Ridge. The lower variances to the north of that ridge in the center of the basin are in a region of smoother bathymetry, and again the dominant vertical wavelengths (Figure 5) tend to be longer there, consistent with propagation from remote forcing areas of most internal waves and weaker mixing found in that region.

Moving northward in the Pacific, mean deep w' variances (Figure 4) are substantially higher than average within and immediately north of the Samoan Passage and in the Penrhyn Basin east of the Manihiki Plateau. The Samoan Passage is a constriction for northward flow of bottom water into the rest of the Pacific, with hydraulic jumps and strong mixing observed locally (Carter et al., 2019). The high values continuing farther to the north of the Passage and east of the Manihiki Plateau are perhaps partly owing to relatively rough bathymetry in those regions. Values are also high for the few floats in the North Pacific, all of which are close to steep topography. Moving from South to North these floats are found in the Clarion-Clipperton Fracture Zone, around the Hawaiian Islands, and off the continental slope just west of San Diego.

4. Summary and discussion

Internal wave signatures are apparent in variations of descent rate data (w') from Deep SOLO floats. Mean deep w' variances (Figure 4) and dominant vertical wavelengths (Figure 5) exhibit geographical variability tied to proximity to rough seafloor topography and deep currents, with variations among and even within some deep basins. For example, within the Brazil Basin, mean deep w' variances in the western part of the basin, where bottom roughness is very low on the abyssal plain, are on average about 3 times lower than those in the eastern part of the basin, where topography is very rough on the western flank of the Mid-Atlantic Ridge. This result is consistent with earlier findings of increased microscale energy and mixing over mid-ocean ridges (Polzin et al., 1997). Another interesting contrast in mean deep w' variances is the relatively high values found within the Samoan Passage compared to the lower values immediately to the south of that passage. This elevated activity could be partly owing to the influence of lee waves and hydraulic jumps as bottom water flows

northward through the passage (Carter et al., 2019). The elevated mean deep w' variances further north of the passage could also be partly owing to the interactions of tidal flows, which can propagate over long distances, especially those at low vertical modes (Zhao et al., 2016), with local rough bathymetry.

Overall, mean deep w' variances are correlated at 0.16 with local topographic roughness. So, as expected, internal wave activity is higher in the vicinity of rough topography. While this correlation is not extremely high, it is easily statistically significant (p=0.00). Furthermore, the dominant vertical wavelengths of w' are also correlated at -0.07 with local topographic roughness (again, with p=0.00). This statistically significant negative correlation is also expected as locally generated internal waves should have shorter vertical wavelengths than those propagating from more distant generation regions, because the shorter vertical wavelength packets are more subject to breaking and subsequent dissipation.

It would also be interesting to examine internal wave signatures in deep density vertical strain using the float scientific data (temperature, salinity, and pressure profiles), similarly to what has been done with core Argo data (Whalen et al., 2012). However, many of these Deep SOLO floats were set to sample at 50 dbar intervals over some of the deeper portions of the water column to conserve float battery energy, and sampling at more frequent intervals field (25 dbar would be sufficient) would be required to properly estimate the deep strain. Nonetheless, the data we have so far of deep w' variances provides a tantalizing glimpse of what might be learned of internal wave energy distributions in the deep ocean from a global Deep Argo array. Already, with only a few Deep Argo regional pilot arrays established, there are roughly three times the number of Deep Argo profiles than were used from all of WOCE in one study of deep mixing (Kunze et al., 2006).

Since float profiling rates typically take tens of seconds to adjust to changes in forcing including ambient vertical velocity, float buoyancy, and ambient density (e.g., Cusack et al., 2017), the perturbations in their descent rates will be slightly attenuated and lagged relative to the actual internal wave vertical velocities. However, even for the shortest dominant vertical wavelengths (e.g. 393 dbar) and the fastest background float descent rates (e.g. 0.17 dbar s^{-1}), profiling for half a vertical wavelength would take around 20 minutes, far longer than float adjustment times. Hence, these measurement errors should have a very small impact on the results of this study.

For internal waves generated at the sea-floor, which would have group velocity (and energy) propagation upward, hence phase velocity (crest and troughs) propagation downward, sampling on descent would bias vertical wavelength estimates towards long values. For such internal waves at the inertial period, the dominant vertical wavelengths estimated here would be biased long by 10 (±6) %. If instead the energy propagation were always downward, the wavelength estimates would be biased short by 8 (±4) % at inertial periods. For internal waves with periods shorter than inertial, these errors would be larger. However,

if energy propagation were evenly split between upward and downward packets, these errors would instead be random, and unbiased. At any rate, wave amplitudes should be unaffected by this issue.

Acknowledgments and Data Availability Statement

References

Alford, M. H., MacKinnon, J. A., Simmons, H. L., & Nash, J. D. (2016). Near-Inertial Internal Gravity Waves in the Ocean. *Annual Review of Marine Science, Vol 8, 8*, 95–123. https://doi.org/10.1146/annurev-marine-010814-015746

Carter, G. S., Voet, G., Alford, M. H., Girton, J. B., Mickett, J. B., Klymak, J. M., et al. (2019). A Spatial Geography of Abyssal Turbulent Mixing in the Samoan Passage. *Oceanography, 32*(4), 194–203. https://doi.org/10.5670/oceanog.2019.425

Cleveland, W. S., & Devlin, S. J. (1988). Locally Weighted Regression - An Approach to Regression-Analysis by Local Fitting. *Journal of the American Statistical Association, 83*(403), 596–610. https://doi.org/10.1080/01621459.1988.10478639

Cusack, J. M., Garabato, A. C. N., Smeed, D. A., & Girton, J. B. (2017). Observation of a Large Lee Wave in the Drake Passage. *Journal of Physical Oceanography, 47*(4), 79—810. https://doi.org/10.1175/JPO-D-16-0153.1

Danioux, E., Klein, P., & Riviere, P. (2008). Propagation of Wind Energy into the Deep Ocean through a Fully Turbulent Mesoscale Eddy Field. *Journal of Physical Oceanography, 38*(10), 2224–2241. https://doi.org/10.1175/2008JPO3821.1

de Lavergne, C., Madec, G., Le Sommer, J., Nurser, A. J. G., & Naveira Garabato, A. C. (2016). On the Consumption of Antarctic Bottom Water in the Abyssal Ocean, *Journal of Physical Oceanography, 46*(2), 635–661. https://doi.org/10.1175/JPO-D-14-0201.1

de Lavergne, C., Falahat, S., Madec, G., Roquet, F., Nycander, J., & Vic, C. (2019). Toward Global Maps of Internal Tide Energy Sinks. *Ocean Modelling, 137*, 52–75. https://doi.org/10.1016/j.ocemod.2019.03.010

Fer, I., Bosse, A., Ferron, B., & Bouruet-Aubertot, P. (2018). The Dissipation of Kinetic Energy in the Lofoten Basin Eddy. *Journal of Physical Oceanography, 48*(6), 1299–1316. https://doi.org/10.1175/JPO-D-17-0244.1

Foppert, A., Rintoul, S. R., Purkey, S. G., Zilberman, N., Kobayashi, T., Sallèe, J.-B., et al. (2021). Deep Argo Reveals Bottom Water Properties and Pathways in the Australian-Antarctic Basin. *Journal of Geophysical Research: Oceans*, 126, e2021JC017935. https://doi.org/10.1029/2021JC017935

Fu, L. (2007). Interaction of Mesoscale Variability with Large-Scale Waves in the Argentine Basin. *Journal of Physical Oceanography, 37(3)*, 787–793. https://doi.org/10.1175/JPO2991.1

Garrett, C., & Munk, W. (1979). Internal Waves in the Ocean. *Annual Review of Fluid Mechanics, 11*, 339–369. https://doi.org/10.1146/annurev.fl.11.010179.002011

GEBCO Compilation Group (2021) GEBCO 2021 Grid (doi:10.5285/c6612cbe-50b3-0cff-e053-6c86abc09f8f)

Johnson, G. C., Cadot, C., Lyman, J. M., MeTaggart, K. E., & Steffen, E. L. (2020). Antarctic Bottom Water Warming in the Brazil Basin: 1990s Through 2020, From WOCE to Deep Argo. *Geophysical Research Letters, 47(18)*, e2020GL089191. https://doi.org/10.1029/2020GL089191

Johnson, G. C., Lyman, J. M., & Purkey, S. G. (2015). Informing Deep Argo Array Design Using Argo and Full- Depth Hydrographic Section Data. *Journal of Atmospheric and Oceanic Technology, 32*(11), 2187–2198. https://doi.org/10.1175/JTECH-D-15-0139.1

Johnson, G. C., Purkey, S. G., Zilberman, N. V., & Roemmich, D. (2019). Deep Argo Quantifies Bottom Water Warming Rates in the Southwest Pacific Basin. *Geophysical Research Letters, 46*(5), 2662–2669. https://doi.org/10.1029/2018GL081685

Kunze, E. (1985). Near-Inertial Wave-Propagation in Geostrophic Shear. *Journal of Physical Oceanography, 15*(5), 544–565. https://doi.org/10.1175/1520-0485(1985)015<0544:NIWPIG>2.0.CO;2

Kunze, E. (1995). The Energy-Balance in a Warm-Core Ring's Near-Inertial Critical Layer. *Journal of Physical Oceanography, 25*(5), 942–957. https://doi.org/10.1175/1520-0485(1995)025<0942:TEBIAW>2.0.CO;2

Kunze, E. (2017). Internal-Wave-Driven Mixing: Global Geography and Budgets. *Journal of Physical Oceanography, 47*(6), 1325–1345. http://dx.doi.org/10.1175/jpo-d-16-0141.1

Kunze, E., Firing, E., Hummon, J. M., Chereskin, T. K., & Thurnherr, A. M. (2006). Global Abyssal Mixing Inferred from Lowered ADCP Shear and CTD Strain Profiles. *Journal of Physical Oceanography, 36*(8), 1553–1576. https://doi.org/10.1175/JPO2926.1

Munk, W, & Wunsch, C. (1998). Abyssal Recipes II: Energetics of Tidal and Wind mixing. *Deep Sea Research I, 45*(12), 1977–2010. https://doi.org/10.1016/S0967-0637(98)00070-3

Nikurashin, M., & Ferrari, R. (2013). Overturning Circulation Driven by Breaking Internal Waves in the Deep Ocean. *Geophysical Research Letters, 40*(12), 3133–3137. https://doi.org/10.1002/grl.50542

Polzin, K. L., Toole, J. M., Ledwell, J. R., & Schmitt, R. W. (1997). Spatial Variability of Turbulent Mixing in the Abyssal Ocean. *Science, 276*(5309), 93–96. https://doi.org/10.1126/science.276.5309.93

Roemmich, D., Alford, M. H., Claustre, H., Johnson, K., King, B., Moum, J., et al. (2019). On the Future of Argo: A Global, Full-Depth, Multi-Disciplinary Array. *Frontiers in Marine Science, 6*(439). Review. https://doi.org/10.3389/fmars.2019.00439

Roemmich, D., Sherman, J. T., Davis, R. E., Grindley, K., McClune, M., Parker, C. J., et al. (2019). Deep SOLO: A Full-Depth Profiling Float for the Argo Program. *Journal of Atmospheric and Oceanic Technology, 36*(10), 1967–1981. https://doi.org/10.1175/JTECH-D-19-0066.1

Smith, W. H. F., & Sandwell, D. T. (1997). Global Sea Floor Topography from Satellite Altimetry and Ship Depth Soundings. *Science, 277*(5334), 1956–1962. https://doi.org/10.1126/science.277.5334.1956

Thomas, G., Purkey, S. G., Roemmich, D., Foppert, A., & Rintoul, S. R. (2020). Spatial Variability of Antarctic Bottom Water in the Australian Antarctic Basin From 2018–2020 Captured by Deep Argo. *Geophysical Research Letters, 47*(23), e2020GL089467. https://doi.org/10.1029/2020GL089467

Torrence, C., & Compo, G. P. (1998). A Practical Guide to Wavelet Analysis. *Bulletin of the American Meteorological Society, 79*(1), 61–78. https://doi.org/10.1175/1520-0477(1998)079<0061:APGTWA>2.0.CO;2

Waterhouse, A. F., MacKinnon, J. A., Nash, J. D., Alford, M. H., Kunze, E., Simmons, H. L., Polzin, K. L., St. Laurent, L. C., Sun, O. M., Pinkel, R., Talley, L. D., Whalen, C. B., Huussen, T. N., Carter, G. S., Fer, I., Waterman, S., Naveira Garabato, A. C., Sanford, T. B., & Lee, C. M. (2014). Global Patterns of Diapycnal Mixing from Measurements of the Turbulent Dissipation Rate. *Journal of Physical Oceanography, 44*(7), 1854–1872. https://doi.org/10.1175/JPO-D-13-0104.1.

Waterman, S., Garabato, A. C. N., & Polzin, K. L. (2013). Internal Waves and Turbulence in the Antarctic Circumpolar Current. *Journal of Physical Oceanography, 43*(2), 259–282. https://doi.org/10.1175/JPO-D-11-0194.1

Whalen, C. B., Talley, L. D., & MacKinnon, J. A. (2012). Spatial and Temporal Variability of Global Ocean Mixing Inferred from Argo Profiles. *Geophysical Research Letters, 39*, L18612. https://doi.org/10.1029/2012GL053196

Young, W. R., & BenJelloul, M. (1997). Propagation of Near-Inertial Oscillations Through a Geostrophic Flow. *Journal of Marine Research, 55*(4), 735–766. https://doi.org/10.1357/0022240973224283

Zhao, Z. X., Alford, M. H., Girton, J. B., Rainville, L., & Simmons, H. L. (2016). Global Observations of Open-Ocean Mode-1 M-2 Internal Tides. *Journal of Physical Oceanography, 46*(6), 1657–1684. https://doi.org/10.1175/JPO-D-15-0105.1

Zilberman, N. V., Roemmich, D. H., & Gilson, J. (2020). Deep-Ocean Circulation in the Southwest Pacific Ocean Interior: Estimates of the Mean Flow and Variability Using Deep Argo Data. *Geophysical Research Letters, 47*(13), e2020GL088342. https://doi.org/10.1029/2020GL088342
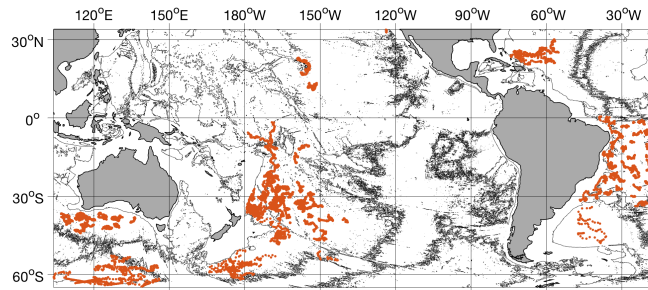
Figure 1. Location of the 10070 Deep SOLO profiles (orange dots) analyzed here with the 4000-m isobath from ETOPO2 (black contours) (Smith & Sandwell, 1997).
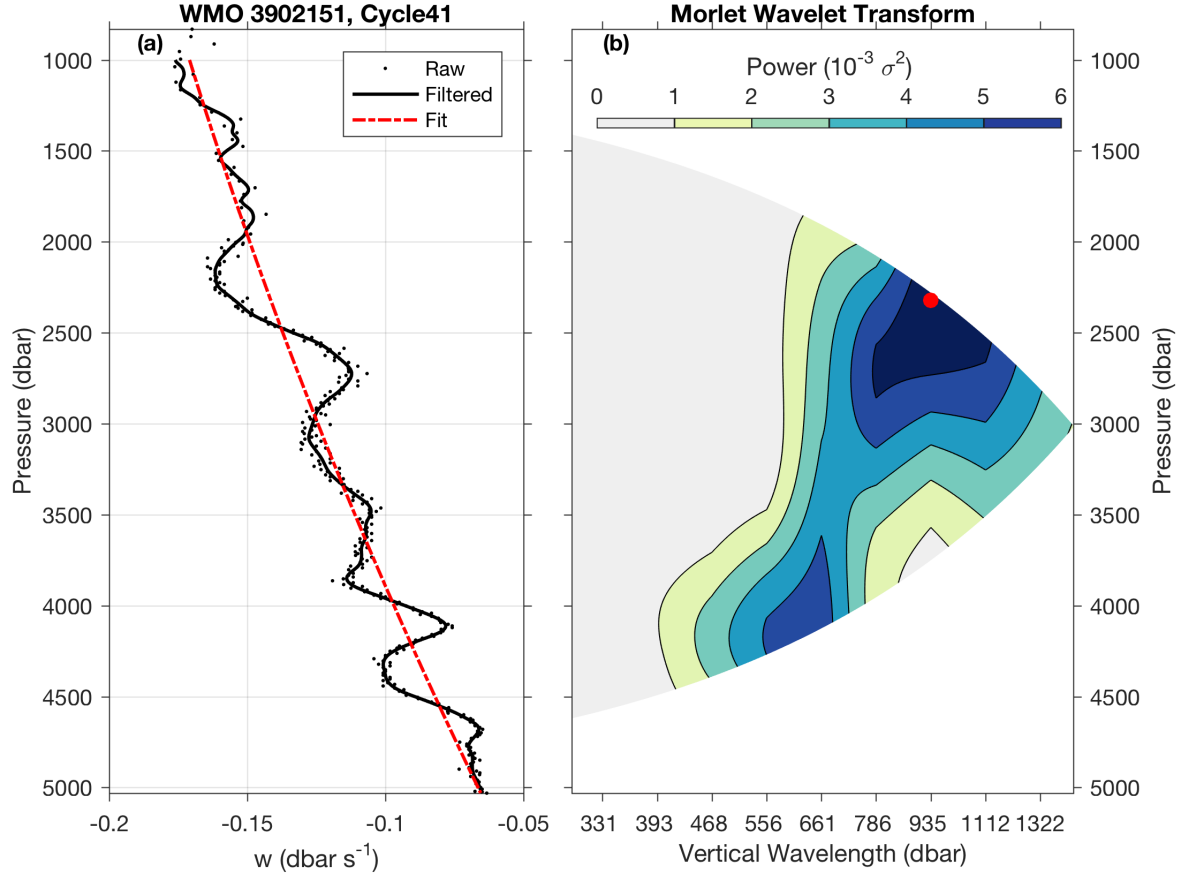
Figure 2. (a) Descent rate of float WMO 3902151 at cycle 41, located on the western flank of the Mid-Atlantic Ridge in the Brazil Basin. Raw values from first differences of pressure over time (black dots), values at 10 dbar intervals derived by filtering raw values with a 150-dbar lengthscale Loess smoother (black curve), and background values (red dashed line) estimated from a 2$^{\text{nd}}$ order polynomial fit to the filtered values vs. pressure for 1000 dbar to the bottom value. (b) Power spectrum for the Morlet wavelet transform of the residual w' (filtered minus background) vertical velocity from panel (a) with contours at uniform intervals and the location of the maximum of the power spectrum (large red dot), disregarding values in the "cone of influence" affected by zero-padding of edge values (which has been masked with white in the figure).
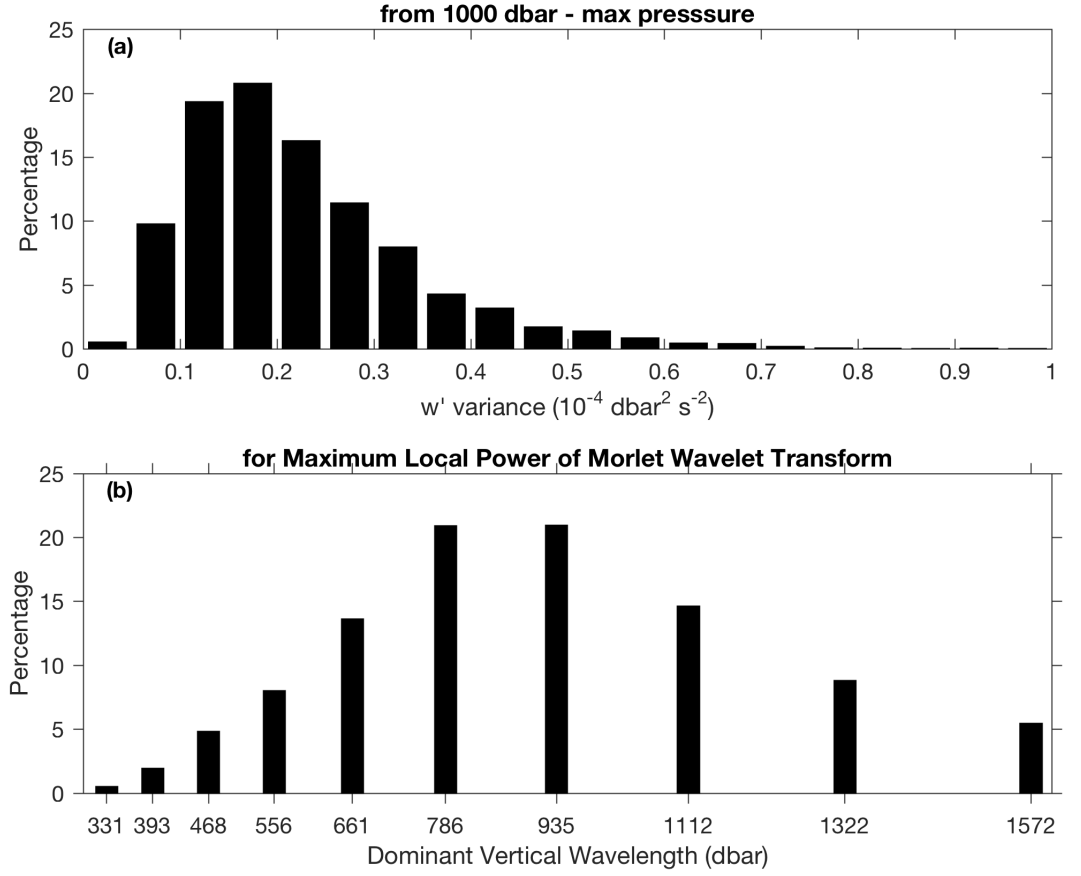
Figure 3. Histograms of (a) mean deep *w'* variance and (b) w' dominant vertical wavelength in Morlet wavelet power spectra of *w'* from 1000 dbar to the maximum pressures of the 10070 Deep SOLO profiles analyzed.
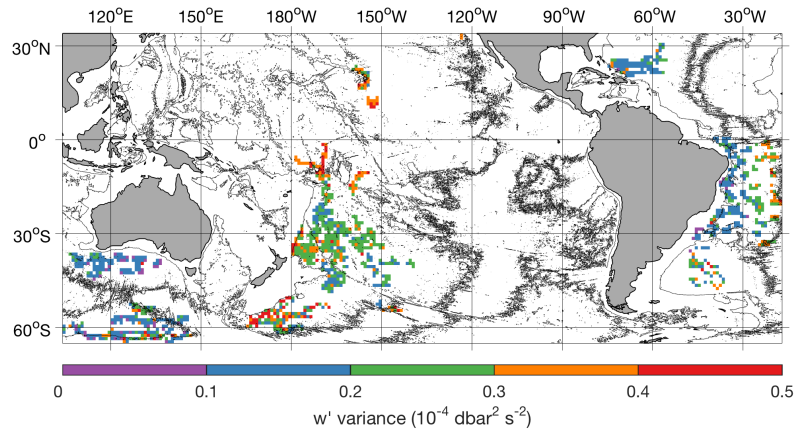
Figure 4. Mean deep w' variances from 1000 dbar to the bottom pressure of deep SOLO profiles averaged in 1° lat. × 1° long bins (colorbar at 0.1×10^{-4} dbar^2 s^{-2} intervals).
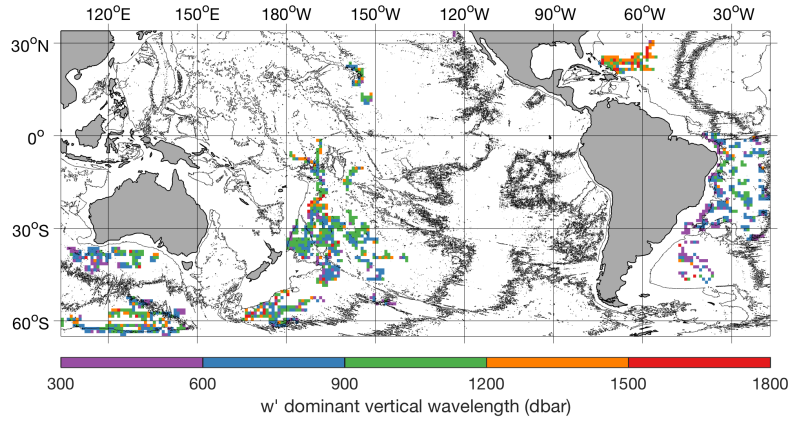
Figure 5. Dominant vertical wavelengths of w' from 1000 dbar to the bottom pressure of deep SOLO profiles averaged in 1° lat. × 1° long bins (colorbar at 300 dbar intervals).